J Solid State Electrochem (2010) 14:17–26
DOI 10.1007/s10008-008-0772-3

ORIGINAL PAPER

Synthesis and surface treatment of $LiNi_{1/3}Co_{1/3}Mn_{1/3}O_2$ cathode materials for Li-ion batteries

George Ting-Kuo Fey · Chung-Sheng Chang · T. Prem Kumar

Received: 15 September 2008 / Revised: 24 November 2008 / Accepted: 14 December 2008 / Published online: 20 January 2009

Abstract In order to shorten process time and possibly reduce synthesis cost of $LiNi_{1/3}Co_{1/3}Mn_{1/3}O_2$, the cathode material was prepared by solution combustion and microwave synthesis routes with reduced duration of calcination. The products were also surface-modified with Al_2O_3 by a mechano-thermal coating process to enhance cyclability. The structure and morphology of the bare and the surface-modified $LiNi_{1/3}Co_{1/3}Mn_{1/3}O_2$ samples were characterized by X-ray diffraction, field-emission scanning electron microscopy, transmission electron microscopy, energy-dispersive spectroscopy, and differential scanning calorimetry techniques. At a 0.1-C rate and between 4.6 and 2.5 V, the products delivered a first-cycle discharge capacity of as much as 195 mA h/g. Surface modification of $LiNi_{1/3}Co_{1/3}Mn_{1/3}O_2$ with alumina resulted in improved cyclability.

Keywords $LiNi_{1/3}Co_{1/3}Mn_{1/3}O_2$ · Solution combustion method · Microwave synthesis · Mechano-thermal coating · Coated cathodes · Lithium-ion battery

Introduction

Layered oxides of the type $Li[Co–Ni–Mn]O_2$ have recently been shown to possess several superior characteristics as compared to those of the individual layered compounds, $LiMO_2$ (M = Co, Ni, or Mn), in terms of performance, economy, thermal stability, non-toxicity, etc. [1]. Typical compositions that have been investigated include $LiNi_{0.8}Co_{0.2}O_2$ [2], $LiNi_{0.5}Co_{0.5}O_2$ [3], $LiNi_xCo_{1-2x}Mn_xO_2$ [4] and $LiNi_{0.6}Co_{0.4-x}Mn_xO_2$ [5]. Additionally, doping with non-transition metal ions as a method to improve the electrochemical and safety characteristics of cathode materials has also gained much interest. For example, $LiCoO_2$ doped with Al^{3+} [6, 7] and $LiNi_{0.75}Co_{0.25}O_2$ doped with Mg^{2+} [8] have been shown to improve cyclability and safety. In 2001, Ohzuku and Makimura [9] suggested $LiCo_{1/3}Mn_{1/3}O_2$ as an alternative to the popular $LiCoO_2$ cathode. However, because the valence states of nickel, cobalt, and manganese in the compound are suggested as +2, +3, and +4, respectively [10, 11], this is not a true solid solution of the end members, $LiMO_2$, where the transition metals are in their trivalent states. $Li[Ni_{1/3}Co_{1/3}Mn_{1/3}]O_2$ has been shown to deliver a specific capacity of 160 mA h/g between 2.5 and 4.4 V [11]. Moreover, in its oxidized state, it is less oxidative towards the electrolyte than $LiCoO_2$ or $LiNiO_2$ [12]. Thus, $Li[Ni_{1/3}Co_{1/3}Mn_{1/3}]O_2$ is considered as a promising next-generation cathode material.

Preparation of $LiNi_{1/3}Co_{1/3}Mn_{1/3}O_2$ can be effected by a number of methods including coprecipitation [13], sol-gel [14], solid-state [15], solution [16], mixed hydroxide [17], hydrothermal [18], water-in-oil emulsion [19], and ultrasonic spray pyrolysis [20] methods. The most popular method is the coprecipitation method. Although preparation via hydroxide coprecipitation leads to phase-pure products [21], the method is generally considered cumbersome [11, 13]. With an aim to shorten process time and possibly reduce synthesis cost, we adopted two synthesis procedures for $LiNi_{1/3}Co_{1/3}Mn_{1/3}O_2$: solution combustion with hexamethylenetetramine (HMTA) as a fuel and microwave

G. Ting-Kuo Fey (✉) · C.-S. Chang
Department of Chemical and Materials Engineering,
National Central University,
Chung-Li, Taiwan 32054, Republic of China
e-mail: gfey@cc.ncu.edu.tw

T. P. Kumar
Electrochemical Power Systems Division,
Central Electrochemical Research Institute,
Karaikudi 630006 Tamil Nadu, India

synthesis followed by short-duration high-temperature calcination.

The cyclability of electrode materials is greatly dependent on changes in lattice dimensions of the host material and, therefore, to volume changes during charging and discharging. In other words, materials that undergo zero strain [22] or zero-volume change [23] should be ideal as long-cycling electrode materials. Because such a property cannot be expected with all battery-active materials, surface modifications that suppress volume changes have gained popularity [24–28]. In the present case, surface coating with alumina by a mechano-thermal coating procedure developed in our laboratory [29–31] was adopted to improve the cyclability of the cathode material.

Experimental

$LiNi_{1/3}Co_{1/3}Mn_{1/3}O_2$ powders were prepared by solution combustion and microwave methods. Coating of the products with alumina was done by a mechano-thermal technique.

Solution combustion method

Stoichiometric amounts of lithium nitrate (Merck, 99%), nickel nitrate (Acros, 99%), cobalt nitrate (Aldrich, 99%), and manganese acetate (Showa, 98%) were dissolved in a minimum quantity of distilled water. The required amount of the fuel HMTA (Riedel-de Haën, 99%), as calculated by the method of Jain et al. [32] was added to this mixture. After stirring for 20 min, the mixture was quickly introduced in a muffle furnace maintained at 400 °C for 30 min. The resulting black powder was then calcined at 950 °C for 15 h in air and slowly cooled to room temperature to get the desired product (hereafter referred to as SC).

Microwave method

A mixture of lithium nitrate, nickel nitrate, cobalt nitrate, and manganese acetate was dispersed in ethanol by a 30-min sonication. Stirring at 70 °C yielded a thick paste, which was pressed into pellets, transferred to a crucible, and subjected to 15 min of microwave irradiation in a domestic microwave oven (SHARP R-341B, 630-W power output). The black powder obtained was subsequently calcined at 950 °C for 1 h to get the final product (designated as MM in this paper). It must be mentioned here that absorption of microwaves by the crucible can alter the intensity of the microwave on the pellet. In the absence of data on the microwave absorption characteristics of the crucible material, it is impossible to assess the way different regions of the pellet get irradiated. We have, therefore, not addressed this problem in this study.

Al_2O_3 coating

The cathode particles were coated with alumina by a mechano-thermal technique [29–31]. A dispersion of nanoparticles of Al_2O_3 was obtained by a 10-h sonication in ethanol to which $LiNi_{1/3}Co_{1/3}Mn_{1/3}O_2$ (SC or MM) was added such that the weight ratios of $LiNi_{1/3}Co_{1/3}Mn_{1/3}O_2$ to Al_2O_3 were 99.75:0.25, 99.50:0.50, 99.00:1.00, and 98.50:1.50. The mixture was initially sonicated for 1 h and then stirred on a magnetic stirrer for 10 h. Evaporation of the solvent at 60 °C gave cathode particles coated with alumina. A 10-h calcination at 450 °C in air ensured complete adhesion of the coated particles with the core material [29–31, 33].

Structural and morphological characterization

Structural analysis of the pristine and coated samples was carried out by X-ray diffraction (XRD; Siemens D-5000, Mac Science MXP18). Surface morphology of the coated materials was examined by field-emission scanning electron microscopy (FE-SEM; Hitachi S-800). Microstructures of the coated particles were examined by transmission electron microscopy (TEM; Hitachi HF-2000). Depth profiles of aluminum, nickel, cobalt, manganese, and oxygen in the coated materials were recorded by electron spectroscopy for chemical analysis (ESCA; VG Scientific ESCALAB 250). Thermal stability measurements were carried out by differential scanning calorimetry (DSC; Perkin Elmer DSC 7).

Electrochemical characterization

Coin cells of the 2032 configuration were assembled in an argon-filled VAC MO40-1 glove box in which the oxygen and water contents were maintained below 2 ppm. Lithium metal (Foote Mineral) was used as the anode and a 1-M solution of $LiPF_6$ in EC:DEC (1:1 *v*/*v*; Tomiyama Chemicals) was used as the electrolyte. The cathode was prepared by blade coating a slurry of 85 wt.% bare or coated active material with 10 wt.% conductive carbon black and 5 wt.% poly(vinylidene fluoride) binder in *N*-methyl-2-pyrrolidone on an aluminum foil, drying overnight at 120 °C in an oven, roller pressing the dried coated foil, and punching out circular discs. The cells were cycled at 0.2-C rate (with respect to a theoretical capacity of 274 mA h/g) between 2.5 and 4.6 V on a multi-channel battery tester (Maccor 4000). Phase transitions occurring during the cycling processes were examined by slow-scan cyclic voltammetry performed with a three-electrode glass cell. The working electrodes were prepared by coating both sides of an

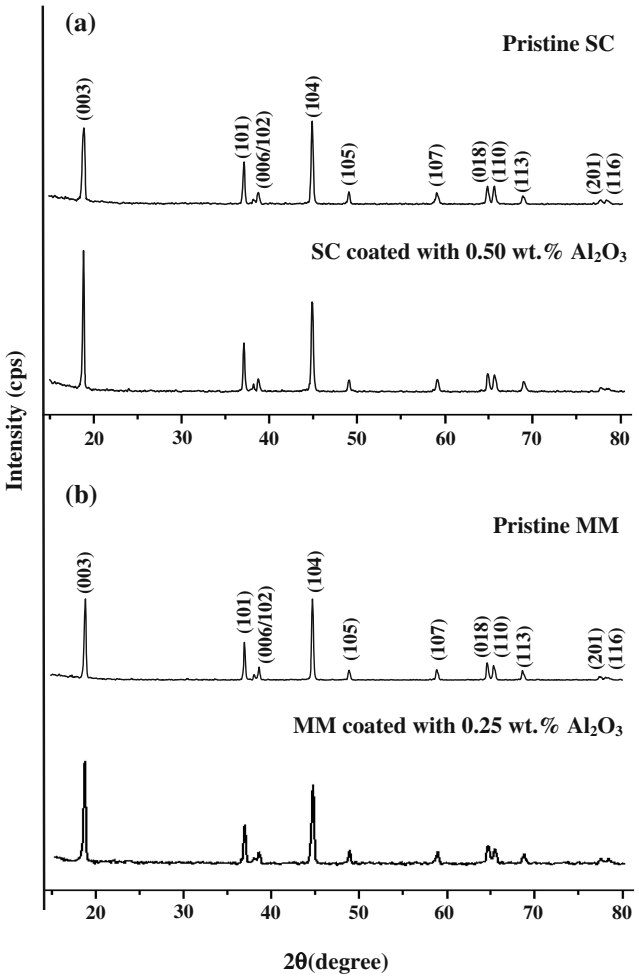

Fig. 1 X-ray diffraction patterns of (*a*) the pristine and 0.50 wt.% Al_2O_3-coated $LiNi_{1/3}Co_{1/3}Mn_{1/3}O_2$-SC and (*b*) the pristine and 0.25 wt.% Al_2O_3-coated $LiNi_{1/3}Co_{1/3}Mn_{1/3}O_2$-MM

aluminum foil with the cathode powder. The cells for cyclic voltammetry were assembled inside the glove box with lithium metal foil serving as both counter and reference electrodes. The electrolyte used was the same as that for the coin cell. Cyclic voltammograms were run on a Solartron 1287 Electrochemical Interface at a scan rate of 0.1 mV/s between 2.5 and 4.7 V.

Results and discussion

X-ray diffraction

Typical X-ray diffraction patterns of pristine and alumina-coated $LiNi_{1/3}Co_{1/3}Mn_{1/3}O_2$ are shown in Fig. 1. Both the bare and alumina-modified samples exhibited diffraction patterns that conform to the R3m symmetry of the core material and identifiable with the hexagonal α-$NaFeO_2$ structure. The patterns are in agreement with that of $LiNi_{1/3}Co_{1/3}Mn_{1/3}O_2$ reported by Ohzuku et al. [9, 12]. The sharp diffraction peaks and the doublets (*006*)/(*102*) and (*018*)/(*110*) indicate a perfect hexagonal lattice ordering in $Li(Ni_{1/3}Co_{1/3}Mn_{1/3})O_2$ [11, 34, 35]. The values of the lattice parameters *a* and *c* given in Tables 1 and 2 are in good agreement with those reported in the literature [11, 34, 36]. Values of more than 4.9 for the *c*/*a* ratios also reveal the well-defined layered structure [11, 37]. The absence of any diffraction patterns corresponding to Al_2O_3 is attributed to the amorphous nature of Al_2O_3 as well as to the small concentration of the coating material [33], which indicates that the presence of the coating did not alter the crystal structure of the core material. However, the lattice constants *a* and *c* of the coated materials differ from those of the bare samples, suggesting the presence of solid solutions formed by the reaction of the Al_2O_3 particles with the core $LiNi_{1/3}Co_{1/3}Mn_{1/3}O_2$. It is possible that, during calcination, a substitutional compound such as $LiAl_y(Ni_{1/3}Mn_{1/3}Co_{1/3})_{1-y}O_2$ could have formed through the interaction of the aluminum species with the substrate [38]. The values of the ratio of intensities I_{003}/I_{104}, which are generally greater than 1, suggest good cation ordering in the samples [39].

According to Dahn and coworkers [40, 41], the *R* factor, defined as the ratio of the intensities of the hexagonal characteristic doublet peaks (*006*) and (*102*) to the (*101*) peak, is an indicator of hexagonal ordering. They suggest that materials with a low *R* factor value had a better hexagonal ordering and, hence, would exhibit better electrochemical characteristics [40, 41]. From Table 1, it can be seen that the values of the *R* factor for the bare SC and MM samples are 0.414 and 0.426, respectively, and that coating with alumina

Table 1 Lattice parameters and *R* factor values of bare and Al_2O_3-coated $LiNi_{1/3}Co_{1/3}Mn_{1/3}O_2$

Route	*a* (Å)	*c* (Å)	*c*/*a*	Unit cell volume (Å^3)	I_{003}/I_{104}	*R* factor
$LiNi_{1/3}Co_{1/3}Mn_{1/3}O_2$ synthesized by SC						
Bare	2.849	14.015	4.919	98.536	0.919	0.414
Coating with 0.50 wt.% Al_2O_3	2.856	14.119	4.943	99.752	1.570	0.401
$LiNi_{1/3}Co_{1/3}Mn_{1/3}O_2$ synthesized by MM						
Bare	2.854	14.015	4.911	98.868	1.002	0.426
Coating with 0.25 wt.% Al_2O_3	2.869	14.423	5.027	102.798	1.290	0.423

Table 2 Lattice parameters and *R* factor values of $LiNi_{1/3}Co_{1/3}Mn_{1/3}O_2$ synthesized with different irradiation times

Irradiation time (min)	*a* (Å)	*c* (Å)	*c*/*a*	Unit cell volume (Å^3)	I_{003}/I_{104}	*R* factor
5	2.880	14.090	4.892	101.194	1.385	0.940
15	2.850	14.045	4.928	98.800	1.368	0.925
25	2.881	14.149	4.912	101.680	1.249	0.777
35	2.857	14.060	4.921	99.388	1.268	0.743
15 (followed by short-duration high-temperature calcination)	2.849	14.015	4.919	98.536	0.919	0.414

reduced the *R* factor values. It will be seen below that the electrochemical behavior of the coated samples generally reflects the above trend in the *R* factor values.

Figure 2 shows the effect of duration of microwave irradiation on the structure of MM. The diffraction peaks show that the product could be formed with even 5 min of irradiation. This suggests that even limited exposure to microwaves can trigger and sustain decomposition reactions. It can be seen from Table 2 that the value of the *R* factor decreased with an increase in the duration of irradiation, suggesting that the longer the duration, the better the hexagonal ordering of the lattice. Moreover, the *R* factor value of the calcined sample was much lower than those of the uncalcined samples, which strongly supports the need for a high-temperature post-preparative calcination step.

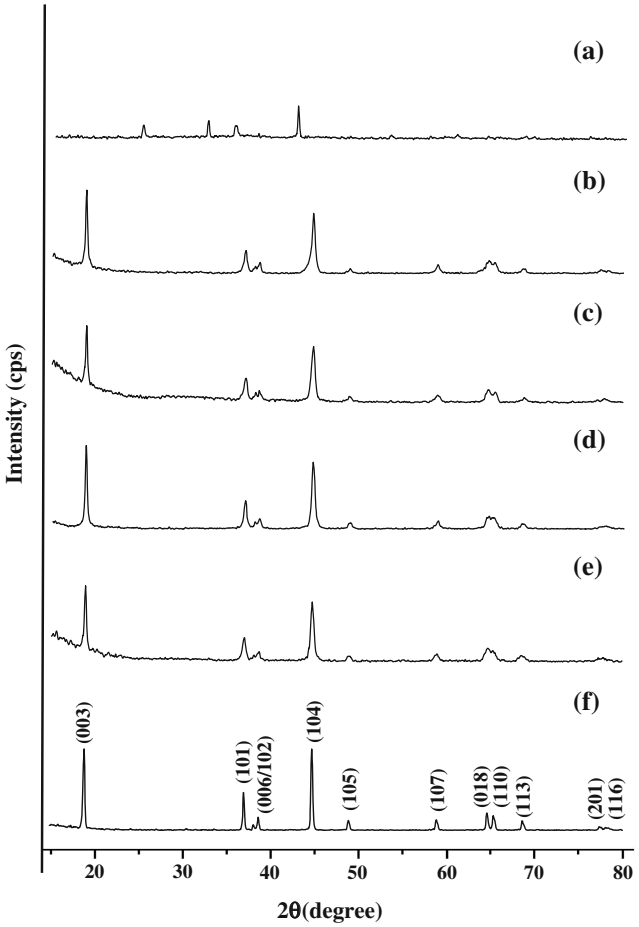

Fig. 2 X-ray diffraction patterns of $LiNi_{1/3}Co_{1/3}Mn_{1/3}O_2$ prepared with different microwave irradiation times: (*a*) 0 min, (*b*) 5 min, (*c*) 15 min, (*d*) 25 min, (*e*) 35 min, and (*f*) 15-min irradiation followed by short-duration high-temperature calcination

Morphology

Typical FE-SEM images of bare and alumina-coated SC powders are shown in Fig. 3. The bare SC shows a fine-grained microstructure with particle size in the range 500–600 nm. However, the texture of the surface of the particles changed upon coating. The increased brightness with increasing coating level is associated with the accumulation of charge on the non-conducting coating material. Moreover, at high coating levels (i.e., beyond a coating level of 0.5 wt.%), small loosely held particles of the coating material begin to appear on the surface, suggesting that the quantities of Al_2O_3 at these levels exceeded what is required to form uniform coatings.

Figure 4 shows an elemental mapping (Ni, Co, Mn, Al, and O) of the 0.5 wt.% alumina-coated SC sample by energy-dispersive spectroscopy (EDS). It can be seen that aluminum is distributed uniformly on the particle surface, suggesting that the mechano-thermal coating process results in good coatings. Figure 5a, b shows TEM images of 0.5 wt.% Al_2O_3-coated SC and 0.25 wt.% Al_2O_3-coated MM samples, respectively. The figures show that Al_2O_3 formed uniform and compact kernels (translucent region) over the $LiNi_{1/3}Co_{1/3}Mn_{1/3}O_2$ particles (dark opaque region), the thickness of the kernels being 15–20 nm.

ESCA

The spatial distributions of Al, Ni, Co, Mn, and O in the 0.5 wt.% Al_2O_3-coated SC sample are displayed in the depth profiles presented in Fig. 6, a and b. As can be seen from Fig. 6, a, the atomic concentrations of Ni, Co, and Mn increase up to depths of about 15 nm and then level off, while that of O dropped up to a depth of about 52 nm. The change in the concentration of aluminum is not very obvious in Fig. 6, a. However, it can be seen from Fig. 6, b, that the

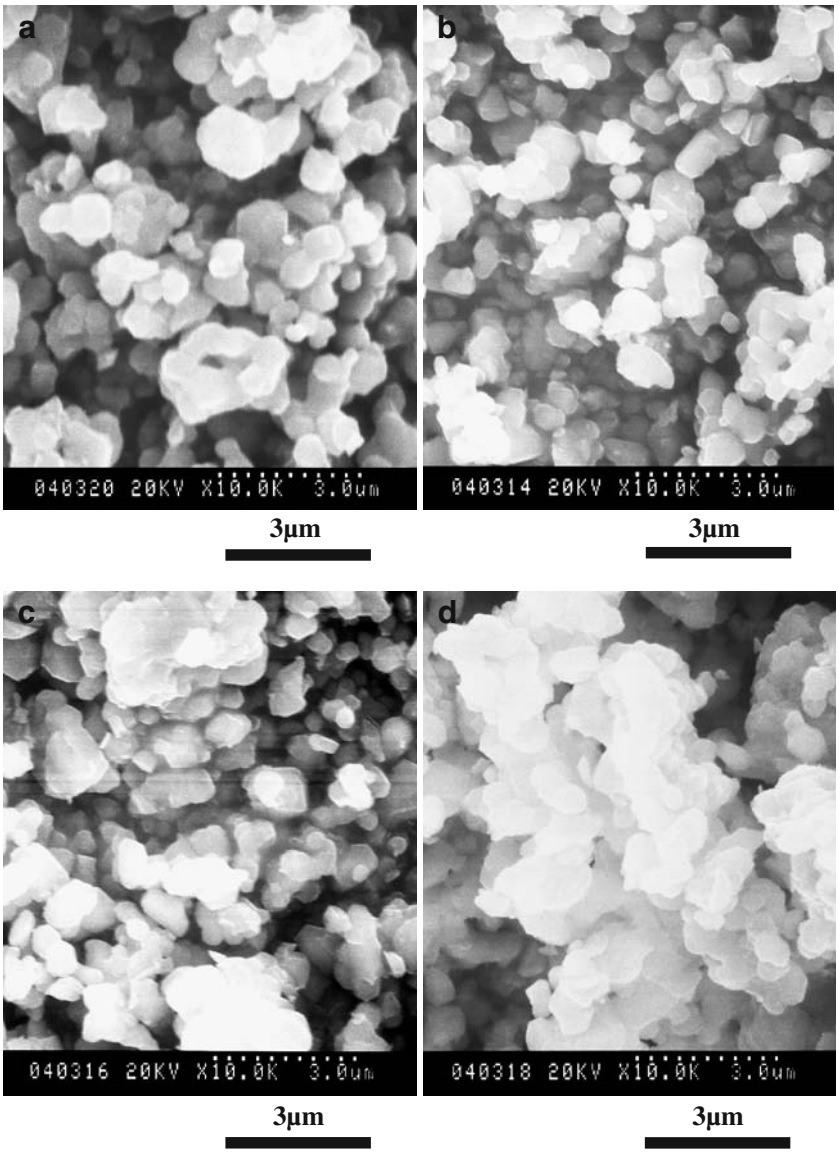

Fig. 3 FE-SEM images of the various weight percent Al_2O_3-coated $LiNi_{1/3}Co_{1/3}Mn_{1/3}O_2$ powders: **a** 0.0, **b** 0.5, **c**1.0, and **d** 1.5 wt.%

concentration of aluminum dropped from 3.2 at.% to nearly 0 at.% at a depth of about 20 nm. The interoxide surface composition on the cathode material must, therefore, be nearly 20 nm thick. This is in agreement with the kernel thickness observed in the TEM image (Fig. 5a).

DSC

In order to compare the thermal stability of $LiNi_{1/3}Co_{1/3}Mn_{1/3}O_2$ synthesized in this study, DSC measurements were performed. Tests were run with both SC and MM samples charged to 4.6 V, and the results were compared with those obtained with $LiCoO_2$ (FMC Corporation) and $LiNi_{0.8}Co_{0.2}O_2$ (FMC Corporation). It can be seen from Fig. 7 that $LiCoO_2$ gives a broad exothermic peak centered at 225 °C, with an onset temperature of 105 °C and releasing 249 J/g. $LiNi_{0.8}Co_{0.2}O_2$ is thermally less stable than $LiCoO_2$ going by the lower-temperature peak around 188 °C, with an onset temperature of 101 °C and releasing higher energy (269 J/g). Compared to these cathode materials, $LiNi_{1/3}Co_{1/3}Mn_{1/3}O_2$ was found to be much more stable: the samples SC and MM gave weak peaks around 306 and 287 °C, respectively. The corresponding exothermic energies were also lower: 120 and 157 J/g. The higher thermal stability of $LiNi_{1/3}Co_{1/3}Mn_{1/3}O_2$ as compared to $LiCoO_2$ [42–44] and $LiNi_{0.8}Co_{0.15}Al_{0.05}O_{2.35}$ [45] has been demonstrated by several groups.

Charge–discharge studies

The first-cycle charge and discharge profiles of the bare $LiNi_{1/3}Co_{1/3}Mn_{1/3}O_2$ samples between 4.6 and 2.5 V at 0.1-

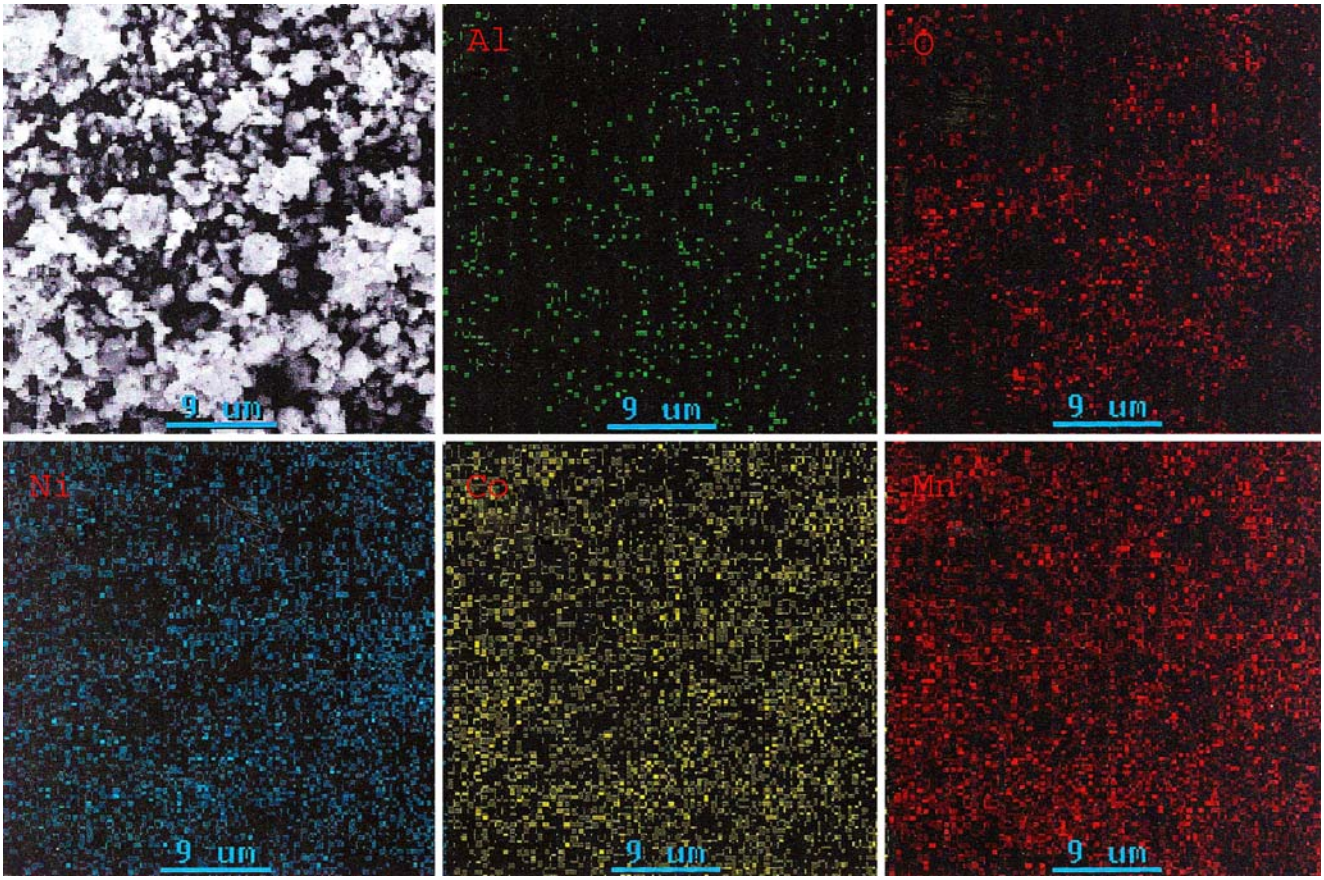

Fig. 4 EDS images of the Al_2O_3-coated $LiNi_{1/3}Co_{1/3}Mn_{1/3}O_2$ powders

C rate are presented in Fig. 8. The first-cycle discharge capacities of the SC and MM samples were 195 and 194 mA h/g, respectively, very much similar to results reported previously [46, 47]. It is noteworthy that the synthesis and processing steps in our study are very simple, fast, convenient, and economical. Figure 9, a and b, shows the cycling behavior of the bare SC and MM samples, respectively, in the ranges 2.5–4.3 and 2.5–4.6 V at 0.2-C rate. For a charging voltage cutoff of 4.3 V, the initial discharge capacities of SC and MM were 147 and 141 mA h/g, respectively. Furthermore, both the samples exhibited excellent cycling stability over 50 cycles. For a higher

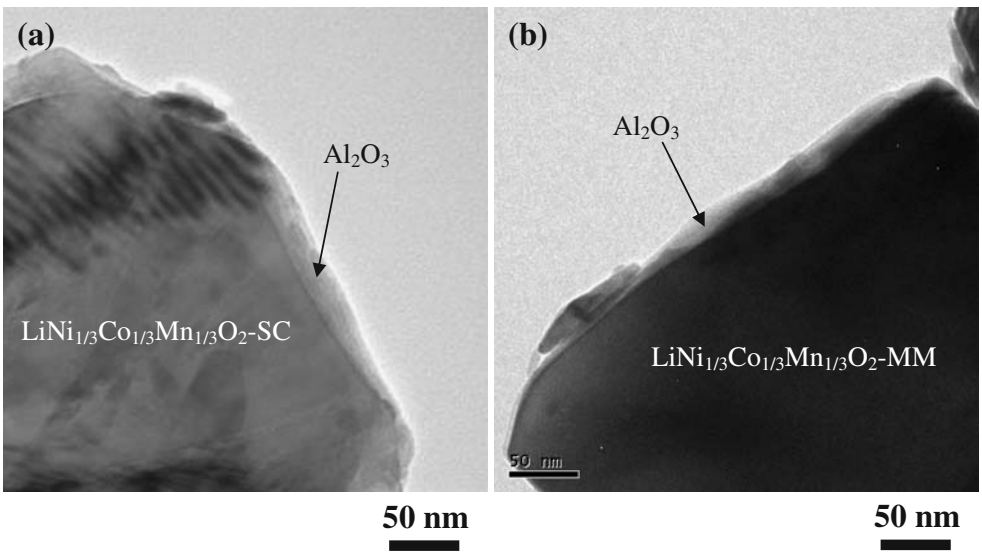

Fig. 5 TEM image of **a** 0.50 wt.% Al_2O_3-coated $LiNi_{1/3}Co_{1/3}Mn_{1/3}O_2$-SC particle and **b** 0.25 wt.% Al_2O_3-coated $LiNi_{1/3}Co_{1/3}Mn_{1/3}O_2$-MM particle

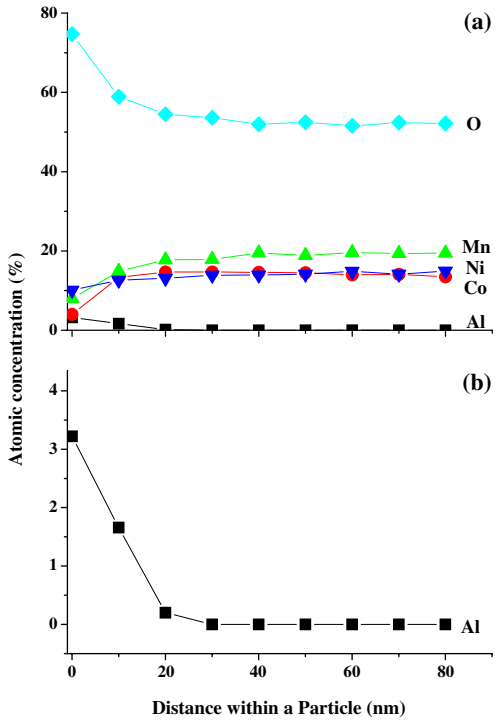

Fig. 6 (*a*) ESCA depth profiles of a $LiNi_{1/3}Co_{1/3}Mn_{1/3}O_2$ particle coated with 0.50 wt.% Al_2O_3 and (*b*) expanded-depth profile of aluminum in the above

charging voltage cutoff of 4.6 V, the first reversible capacities of SC and MM were 179 and 183 mA h/g, respectively, but the attendant capacity fade was rapid. The rapid fade in capacity could suggest detrimental phase transformations at such high voltages. That such fade was not noticed at the lower cutoff of 4.3 V shows that such phase transformations did not occur up to 4.3 V. It is thus clear that limiting the upper charging voltage to 4.3 V would make both the bare $LiNi_{1/3}Co_{1/3}Mn_{1/3}O_2$ materials high-performance and thermally stable cathodes.

Figure 10 depicts the galvanostatic cycling behavior of the alumina-coated SC samples. The cycling was carried out at 0.2-C rate between 2.5 and 4.6 V. The bare sample gave a first-cycle discharge capacity of 179 mA h/g, while the

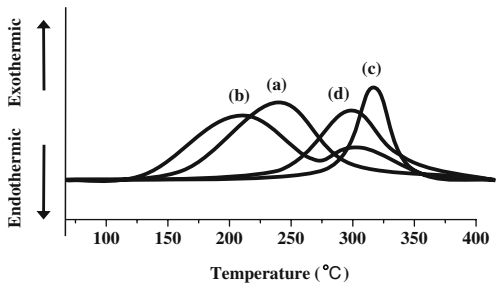

Fig. 7 Differential scanning calorimetry profiles of (*a*) $LiCoO_2$, (*b*) $LiNi_{0.8}Co_{0.2}O_2$, (*c*) $LiNi_{1/3}Co_{1/3}Mn_{1/3}O_2$-SC, and (*d*) $LiNi_{1/3}Co_{1/3}Mn_{1/3}O_2$-MM charged at 4.6 V

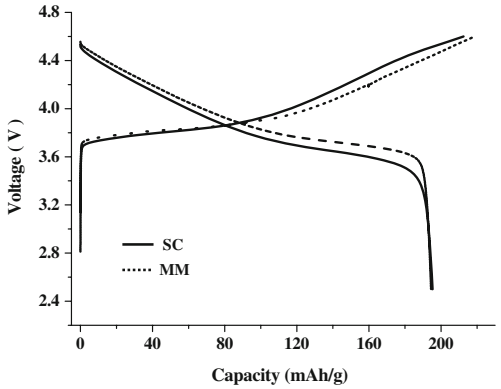

Fig. 8 Initial charge and discharge curves of $LiNi_{1/3}Co_{1/3}Mn_{1/3}O_2$ between 2.5 and 4.6 V at the rate of 0.1-C rate

samples coated with 0.25, 0.50, 1.00, and 1.50 wt.% of Al_2O_3 delivered capacities of 175, 176, 183, and 163 mA h/g, respectively. For an 80% capacity retention, as calculated from the first-cycle discharge capacity of the bare sample, the bare $LiNi_{1/3}Co_{1/3}Mn_{1/3}O_2$ sustained just 47 cycles. It can also be seen from Fig. 10 that the SC product coated with 0.5 wt.% Al_2O_3 gave as many as 97 cycles before reaching the pre-set 80% cutoff in capacity retention. It is inferred that a coating level of less than 0.5 wt.% was insufficient, as reflected in the cycling behavior. However, above a coating level of 0.5 wt.%, the cathode material could be partially

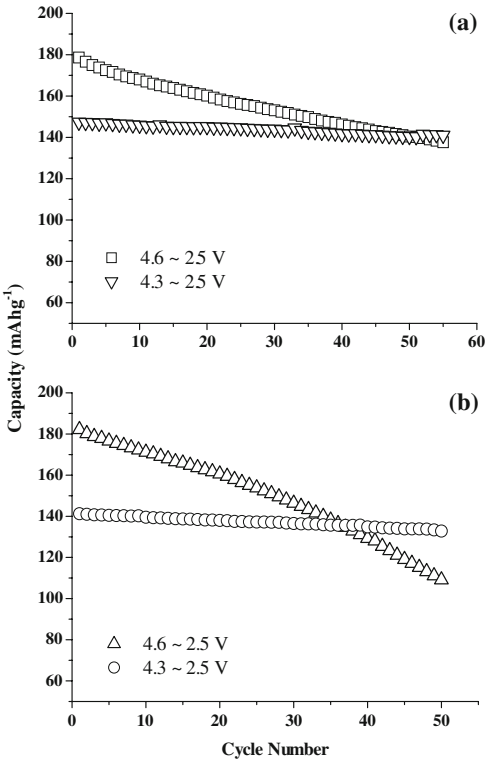

Fig. 9 Galvanostatic cycling performance of the (*a*) $LiNi_{1/3}Co_{1/3}Mn_{1/3}O_2$-SC and (*b*) $LiNi_{1/3}Co_{1/3}Mn_{1/3}O_2$-MM cathode between 2.5~4.3 and 2.5~4.6 V at 0.2-C rate

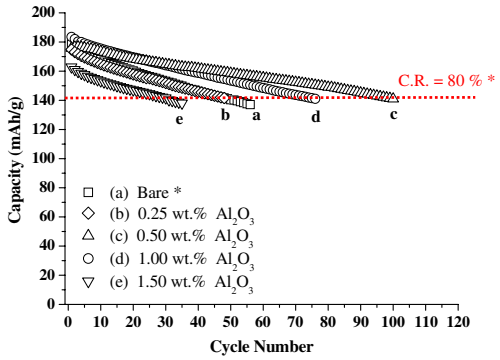

Fig. 10 Cycling behavior of pristine $LiNi_{1/3}Co_{1/3}Mn_{1/3}O_2$-SC and the various weight percent Al_2O_3-coated $LiNi_{1/3}Co_{1/3}Mn_{1/3}O_2$-SC samples. Charge–discharge: 0.2-C rate between 4.6 and 2.5 V

insulated, lowering both cyclability and capacity utilization. The loose particles clinging to the cathode material (Fig. 3) could even prevent particle-to-particle electronic contact.

Figure 11 illustrates the cycling behavior the bare and alumina-coated MM samples. It can be seen from the figure that a coating level of 0.25 wt.% was optimal for obtaining high cyclability. The first-cycle capacities of the bare and the 0.25 wt.% Al_2O_3-coated samples were 183 and 188 mA h/g, respectively. While the coated material sustained 50 cycles before reaching the 80% capacity retention cutoff, the uncoated one could sustain only 30 cycles. Unlike for the SC sample, the enhancement in cyclability for the MM sample was marginal.

Cyclic voltammetry

Improvement in cyclability by surface modification has been attributed to suppression of cycle-limiting phase transitions associated with the intercalation–deintercalation processes by high-fracture-tough coating materials [48] as well as to absence of direct contact of the active material with the electrolyte, limiting the dissolution of the cathode in the electrolyte [26, 49]. Phase transitions during charge–

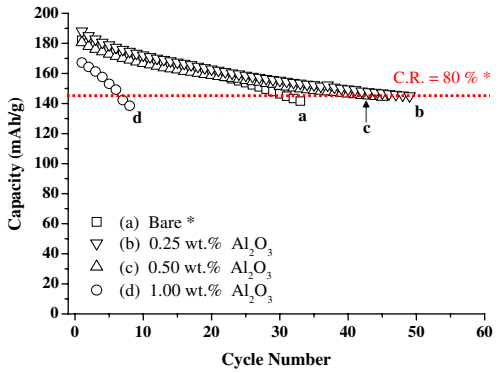

Fig. 11 Cycling behavior of pristine $LiNi_{1/3}Co_{1/3}Mn_{1/3}O_2$-MM and the various weight percent Al_2O_3-coated $LiNi_{1/3}Co_{1/3}Mn_{1/3}O_2$-MM samples. Charge–discharge: 0.2-C rate between 4.6 and 2.5 V

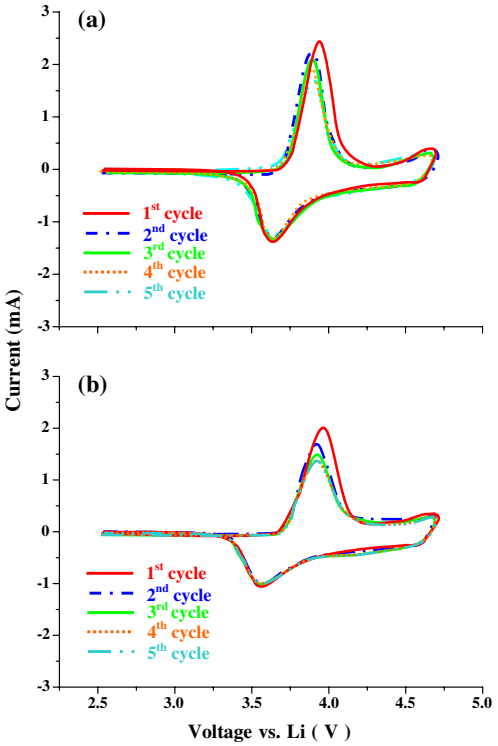

Fig. 12 Cyclic voltammogram of $LiNi_{1/3}Co_{1/3}Mn_{1/3}O_2$/Li cell between 2.5 and 4.7 V at a scan rate of 0.1 mV/s: (*a*) SC and (*b*) MM

discharge processes can be discerned through cyclic voltammetry [50]. However, the cyclic voltammograms recorded with SC and MM between 2.5 and 4.7 V at a scanning rate of 0.1 mV/s (Fig. 12) showed neither evidence of current peaks ascribable to phase transitions nor of their suppression. In fact, Yabuuchi et al. [17] attribute the high capacity, high-rate capability, and excellent cyclability of $LiCo_{1/3}Ni_{1/3}Mn_{1/3}O_2$ to its unique electronic structure and extremely small volume changes upon cycling.

Figure 12, a, recorded with SC shows a sharp and intense peak at 3.92 V and a diminutive peak around 4.62 V in the first scan. The corresponding cathodic peaks can be seen at 3.61 and 4.54 V. From the second scan onwards, the anodic peaks shift to 3.86 and 4.62 V, respectively. Similarly, the MM sample gave an intense peak at 3.91 V and a weak peak around 4.67 V in the first scan, with the corresponding cathodic peaks at 3.55 and 4.67 V. In the subsequent scans, the anodic peaks can be seen shifted to 3.89 and 4.67 V. No shift can be noticed with the cathodic peaks. This behavior is believed to be due to initial activation and stabilization [51]. This also indicates the formation of a solid electrolyte interphase in the first scan [52]. According to Shaju et al. [11], the anodic peak around 3.9 V arises due to oxidation of Ni^{2+} to Ni^{4+} and the one near 4.5 V is related to the Co^{4+}/Co^{3+} couple. However, Shin et al. [46] suggest that the oxidation of nickel proceeds in two successive steps,

$Ni^{2+} \rightarrow Ni^{3+} \rightarrow Ni^{4+}$, via Ni^{3+}, rather than in a single step, $Ni^{2+} \rightarrow Ni^{4+}$. Accordingly, potential assignments would be: Ni^{2+}/Ni^{3+} (3.7–3.9 V), Ni^{3+}/Ni^{4+} (3.9–4.4 V), and Co^{3+}/Co^{4+} (4.4–4.6 V). Manganese has been shown to exist as Mn^{4+} ions in this oxide and does not take part in the redox processes between 2.5 and 4.7 V [53].

Conclusions

$LiNi_{1/3}Co_{1/3}Mn_{1/3}O_2$ cathode materials were prepared by SC and MM methods. The elaboration and subsequent processing are simple, fast, and convenient and require less time for the conventional coprecipitation route. The products were then surface-treated with alumina by a mechano-thermal procedure. XRD results showed that the bare and coated SC and MM samples possessed a typical hexagonal α-$NaFeO_2$ structure. FE-SEM micrographs revealed that, at low coating levels, the alumina particles were uniformly distributed on $LiNi_{1/3}Co_{1/3}Mn_{1/3}O_2$ and that at higher coating levels extra alumina particles got glued to the cathode surface. TEM images showed the presence of alumina as a compact kernel of about 20 nm thick around the cathode. Depth profiles recorded by ESCA substantiated the TEM findings. DSC analysis clearly established the higher thermal stability of $LiNi_{1/3}Co_{1/3}Mn_{1/3}O_2$ as compared to $LiCoO_2$ and $LiNi_{0.8}Co_{0.2}O_2$. The SC and MM products delivered initial discharge capacities of 179 and 183 mA h/g between 4.6 and 2.5 V at 0.2-C rate. Galvanostatic cycling studies showed that, at coating levels of 0.50 wt.% on SC and 0.25 wt.% on MM, the improvement in cyclability was the greatest. The major oxidation peaks around 3.9 and 4.5 V in the cyclic voltammograms were ascribed to the oxidation of Ni^{2+} and Co^{3+}, respectively.

Acknowledgement Financial support for this work was provided by the National Science Council of the Republic of China under contract number NSC-97-ET-7-008-004-ET.

References

1. Shukla AK, Kumar TP (2008) Curr Sci 94:314
2. Fey GTK, Chen JG, Wang ZF, Yang HZ, Kumar TP (2004) Mater Chem Phys 87:246. doi:10.1016/j.matchemphys.2004.05.009
3. Belharouak I, Tsukamoto H, Amine K (2003) J Power Sources 119–121:175. doi:10.1016/S0378-7753(03)00174-5
4. MacNeil DD, Lu ZH, Dahn JR (2002) J Electrochem Soc 149:A1332. doi:10.1149/1.1505633
5. Liao PY, Duh JG, Sheen SR (2005) J Power Sources 143:212. doi:10.1016/j.jpowsour.2004.12.001
6. Myung S, Kumagai N, Komaba S, Chung HT (2001) Solid State Ion 139:47. doi:10.1016/S0167-2738(00)00828-6
7. Yoon WS, Lee KK, Kim KB (2000) J Electrochem Soc 147:2023. doi:10.1149/1.1393479
8. Chang CC, Kim JY, Kumta PN (2000) J Power Sources 89:56. doi:10.1016/S0378-7753(00)00393-1
9. Ohzuku T, Makimura Y (2001) Chem Lett 7:642. doi:10.1246/cl.2001.642
10. Lu Z, MacNeil DD, Dahn JR (2001) Electrochem Solid-State Lett 4(12):200. doi:10.1149/1.1413182
11. Shaju KM, Subba Rao GV, Chowdari BVR (2002) Electrochim Acta 48:145. doi:10.1016/S0013-4686(02)00593-5
12. Yabuuchi N, Ohzuku T (2003) J Power Sources 119–121:171. doi:10.1016/S0378-7753(03)00173-3
13. Sun YK, Cho SW, Lee SW, Yoon CS, Amine K (2007) J Electrochem Soc 154:A168. doi:10.1149/1.2422890
14. Li J, Zhang ZR, Guo XJ, Yang Y (2006) Solid State Ion 177:1509. doi:10.1016/j.ssi.2006.03.055
15. Guo J, Jiao LF, Yuan HT, Wang LQ, Li HX, Zhang M, Wang YM (2006) Electrochim Acta 51:6275. doi:10.1016/j.electacta.2006.04.012
16. Kim JM, Chung HT (2004) Electrochim Acta 49:937. doi:10.1016/j.electacta.2003.10.005
17. Yabuuchi N, Makimura Y, Ohzuku T (2007) J Electrochem Soc 154:A314. doi:10.1149/1.2455585
18. Myung ST, Lee MH, Komaba S, Kumagai N, Sun YK (2005) Electrochim Acta 50:4800. doi:10.1016/j.electacta.2005.02.034
19. Gea TD, Yu LQ, Ni WN, Dong TA, Xing TL, Long HK, Yang JX (2004) Mater Chem Phys 94:423
20. Ju SH, Koo HY, Kim DY, Hong SK, Kang YC, Ha HW, Kim K (2006) J Mater Sci Mater Electron 17:353. doi:10.1007/s10854-006-7470-7
21. Lee MH, Kang YJ, Myung ST, Sun YK (2004) Electrochim Acta 50:939. doi:10.1016/j.electacta.2004.07.038
22. Ohzuku T, Ueda A, Yamamoto N (1995) J Electrochem Soc 142:1431. doi:10.1149/1.2048592
23. Ueda A, Ohzuku T (1994) J Electrochem Soc 141:2010. doi:10.1149/1.2055051
24. Cho J, Kim YJ, Park B (2000) Chem Mater 12:3788. doi:10.1021/cm000511k
25. Mladenov M, Stoyanova R, Zhecheva E, Vassilev S (2001) Electrochem Commun 3:410. doi:10.1016/S1388-2481(01)00192-8
26. Wang Z, Wu C, Liu L, Wu F, Chen L, Huang X (2002) J Electrochem Soc 149:A466. doi:10.1149/1.1456919
27. Fey GTK, Kumar TP (2004) J Ind Eng Chem 10:1090
28. Fey GTK, Lin YY, Kumar TP (2005) Surf Coat Tech 191:68. doi:10.1016/j.surfcoat.2004.06.007
29. Fey GTK, Muralidharan P, Lu CZ, Cho YD (2006) Solid State Ion 177:877. doi:10.1016/j.ssi.2006.01.048
30. Fey GTK, Lu CZ, Kumar TP, Chang YC (2005) Surf Coat Tech 199:22. doi:10.1016/j.surfcoat.2005.03.021
31. Fey GTK, Chen JG, Kumar TP (2005) J Power Sources 146:250. doi:10.1016/j.jpowsour.2005.03.040
32. Jain SR, Adiga KC, Pai Vernekar AR (1981) Combust Flame 40:71. doi:10.1016/0010-2180(81)90111-5
33. Fey GTK, Lu CZ, Kumar TP, Muralidharan P, Chiang AST (2006) J Phys Chem Solids 67:2337. doi:10.1016/j.jpcs.2006.05.023
34. Li DC, Muta T, Zhang LQ, Yoshio M, Noguchi H (2004) J Power Sources 132:150. doi:10.1016/j.jpowsour.2004.01.016
35. Cho TH, Park SM, Yoshio M (2004) Chem Lett 33:704. doi:10.1246/cl.2004.704
36. Jouanneau S, Eberman KW, Krause LJ, Dahn JR (2003) J Electrochem Soc 150:1637. doi:10.1149/1.1622956
37. Cho J, Kim G, Lim HS (1999) J Electrochem Soc 146:3571. doi:10.1149/1.1392516
38. Fey GTK, Chen JG, Kumar TP (2005) J Appl Electrochem 35:177. doi:10.1007/s10800-004-5822-7

39. Kim J, Fulmer P, Manthiram A (1999) Mater Res Bull 34:571. doi:10.1016/S0025-5408(99)00049-5
40. Reimers JN, Rossen E, Jones CD, Dahn JR (1993) Solid State Ion 61:335. doi:10.1016/0167-2738(93)90401-N
41. Dahn JR, Sacken UV, Michal CA (1990) Solid State Ion 44:87. doi:10.1016/0167-2738(90)90049-W
42. Choi J, Manthiram A (2004) Electrochem Solid-State Lett 7: A365. doi:10.1149/1.1792271
43. Ueda A, Uchitomi K, Aoyama S (2003) Electrochemistry Tokyo 71:1214
44. Yoshizawa H, Ohzuku T (2003) ITE Lett 4:569
45. Belharouak I, Sun YK, Liu J, Amine K (2003) J Power Sources 123:247. doi:10.1016/S0378-7753(03)00529-9
46. Shin YJ, Choi WJ, Hong YS, Yoon S, Ryu KS, Chang SH (2006) Solid State Ion 177:515. doi:10.1016/j.ssi.2005.11.019
47. Park SH, Yoon CS, Kang SG, Kim HS, Moon SI, Sun YK (2004) Electrochim Acta 49:557. doi:10.1016/j.electacta.2003.09.009
48. Cho J, Kim YJ, Kim TJ, Park B (2001) Angew Chem Int Ed 40:3367. doi:10.1002/1521-3773(20010917)40:18<3367::AID-ANIE3367>3.0.CO;2-A
49. Wang X, Liu L, Chen L, Huang X (2002) Solid State Ion 148:335. doi:10.1016/S0167-2738(02)00071-1
50. Kavan L, Gratzel M (2002) Electrochem Solid-State Lett 5:A39. doi:10.1149/1.1432783
51. Kim MG, Shin HJ, Kim JH, Park SH, Sun YK (2005) J Electrochem Soc 152:A1320. doi:10.1149/1.1926647
52. Wang Z, Sun YK, Chen L, Huang X (2004) J Electrochem Soc 151:A914. doi:10.1149/1.1740781
53. Kim JM, Chung HT (2004) Electrochim Acta 49:3573. doi:10.1016/j.electacta.2004.03.025